

Validation of an automatic reference region extraction for the quantification of [¹⁸F]DPA-714 in dynamic brain PET studies

Daniel García-Lorenzo^{1,*}, Sonia Lavisso^{2,3,*}, Claire Leroy^{4,5},
 Catriona Wimberley^{4,5}, Benedetta Bodini¹, Philippe Remy^{2,3,7},
 Mattia Veronese⁶, Federico Turkheimer⁶, Bruno Stankoff^{1,8,*}
 and Michel Bottlaender^{4,5,9,*}

Abstract

There is a great need for a non-invasive methodology enabling the quantification of translocator protein overexpression in PET clinical imaging. [¹⁸F]DPA-714 has emerged as a promising translocator protein radiotracer as it is fluorinated, highly specific and returned reliable quantification using arterial input function. Cerebellum gray matter was proposed as reference region for simplified quantification; however, this method cannot be used when inflammation involves cerebellum. Here we adapted and validated a supervised clustering (supervised clustering algorithm (SCA)) for [¹⁸F]DPA-714 analysis. Fourteen healthy subjects genotyped for translocator protein underwent an [¹⁸F]DPA-714 PET, including 10 with metabolite-corrected arterial input function and three for a test–retest assessment. Two-tissue compartmental modelling provided BP_{ND}^{AIF} estimates that were compared to either $BP_{ND}^{LoganSCA}$ or $BP_{ND}^{LoganCRB}$ generated by Logan analysis (using supervised clustering algorithm extracted reference region or cerebellum gray matter). The supervised clustering algorithm successfully extracted a pseudo-reference region with similar reliability using classes that were defined using either all subjects, or separated into HAB and MAB subjects. BP_{ND}^{AIF} , $BP_{ND}^{LoganSCA}$ and $BP_{ND}^{LoganCRB}$ were highly correlated (ICC of 0.91 ± 0.05) but $BP_{ND}^{LoganSCA}$ were ~26% higher and less variable than $BP_{ND}^{LoganCRB}$. Reproducibility was good with 5% variability in the test–retest study. The clustering technique for [¹⁸F]DPA-714 provides a simple, robust and reproducible technique that can be used for all neurological diseases.

Keywords

Inflammation, microglia, positron emission tomography, brain imaging and clinical trials

Received 29 July 2016; Revised 19 December 2016; Accepted 9 January 2017

¹Sorbonne Université, UPMC Paris 06, Institut du Cerveau et de la Moelle Epinière, ICM, Hôpital de la Pitié Salpêtrière, Paris, France

²Commissariat à l'Energie Atomique et aux Energies Alternatives (CEA), Département de Recherche Fondamentale (DRF), Institut d'Imagerie Biomédicale (I2BM), MIRcen, Fontenay-aux-Roses, France

³Centre National de la Recherche Scientifique (CNRS), Université Paris-Sud, Université Paris-Saclay, Neurodegenerative Diseases Laboratory, Fontenay-aux-Roses, France

⁴Commissariat à l'Energie Atomique et aux Energies Alternatives (CEA), Département de Recherche Fondamentale (DRF), Institut d'Imagerie Biomédicale (I2BM), Service Hospitalier Frédéric Joliot, Orsay, France

⁵Imagerie Moléculaire in Vivo, IMIV, CEA, Inserm, CNRS, Univ. Paris-Sud, Université Paris Saclay, Orsay, France

⁶Department of Neuroimaging, Institute of Psychiatry, Psychology and Neuroscience, King's College London, London, UK

⁷Centre Expert Parkinson, Neurologie, CHU Henri Mondor, Assistance Publique Hôpitaux de Paris and Université Paris-Est, Créteil, France

⁸Hôpital Saint Antoine, AP-HP, Paris, France

⁹Commissariat à l'Energie Atomique et aux Energies Alternatives (CEA), Département de Recherche Fondamentale (DRF), Institut d'Imagerie Biomédicale (I2BM), Neurospin, UNIACT, Gif-sur-Yvette, France

*These authors contributed equally to this article.

Corresponding author:

Michel Bottlaender, Neurospin, CEA, 91191 Gif-Sur-Yvette, France.
 Email: michel.bottlaender@cea.fr

Introduction

Neuroinflammation is known to play a key role in the onset and progression of chronic neurodegenerative diseases such as Alzheimer's, Parkinson's and multiple sclerosis. Activated microglia is the main cellular component that characterizes neuroinflammation in these disorders.¹ The availability of a reliable imaging tool aimed at quantifying activated microglia *in vivo* might help to identify specific targets for anti-inflammatory neuroprotective strategies. The translocator protein 18 kDa (TSPO), previously named peripheral benzodiazepine receptor, is only expressed at low levels in the resting brain by quiescent microglial cells, but becomes markedly overexpressed when microglia is activated.²

Although the biological role of TSPO remains poorly understood, with putative effects on cholesterol translocation, steroid synthesis, mitochondrial functioning, and cell apoptosis, it is a promising target for molecular imaging studies of neuroinflammation.^{3,4} The [¹¹C]PK11195 radioligand was the first TSPO tracer used in humans³ and has been investigated in several pilot imaging studies of neuroinflammation in brain diseases.⁵ However, this tracer suffers from serious limitations, such as poor brain penetration and low specific to nonspecific binding ratio in brain and plasma, resulting in a suboptimal signal to noise ratio. Furthermore, the use of ¹¹C radioactive labelling restricts its use to centers with onsite cyclotrons. This has led to the development of second-generation TSPO radiotracers with improved specificity, affinity and signal-to-noise ratio.⁶ However, a drawback for the quantification of second-generation TSPO tracers is related to different binding sites⁷ resulting in three affinity profiles, high-, mixed- and low-affinity binders (HAB, MAB and LAB), which is indicated by the rs6971 single polymorphism contained within the TSPO gene.

Several ¹⁸F-labelled second-generation compounds have been investigated in human and have showed favorable properties for imaging purposes in the brain of healthy subjects.^{8,9} However, among those, [¹⁸F]FEDAA1106 shows slow kinetics, [¹⁸F]FEPPA is rapidly metabolized and [¹⁸F]PBR06 produces brain-penetrant radiolabeled metabolites that could bias the *in vivo* imaging and suitable quantification.^{10,11}

[¹⁸F]DPA-714 provides an improved signal to noise ratio compared to [¹¹C]PK11195 in several preclinical models^{6,12,13} and was identified as one of the most promising TSPO ligands for *in vivo* imaging. The compartmental modeling of [¹⁸F]DPA-714 in the brain of healthy controls has been recently investigated and revealed that the two-tissue compartment model (2-TCM) best described the regional kinetics.^{14,15} Depending on the analyzed region, the V_T (mL/cm³) estimate was about 50% higher in HABs compared to

MABs, supporting the need to take the genetic affinity profile into account for the quantification of this tracer in human studies.¹⁵

For all TSPO radiotracers, there are challenges that relate to the quantification of binding parameters.^{5,16} Compartmental modeling using the arterial input function is classically considered as the gold standard quantification method and was first employed for [¹¹C]PK11195 studies using a 2-TCM with a K_1/k_2 value coupled to be the same across the whole brain cortex.¹⁷

However, arterial blood sampling is an invasive procedure, and therefore a number of alternatives to the standard quantification have been recently proposed. In order to simplify [¹⁸F]DPA-714 quantification, a population-based input function (PBIF) was tested on healthy subjects using one or two arterial or venous samples and compared to the arterial input function (AIF) quantification.¹⁵ A very good agreement between AIF and arterial PBIF was found, but the variability increased when late venous samples were used. In addition, this technique still required an invasive extraction of at least one arterial sample as well as the analysis of the blood metabolites.

Reference region methods have also been applied in several recent [¹¹C]PK11195 clinical studies. Accordingly, the cerebellum has been the main choice as a reference region for TSPO ligands, in particular in ischemic stroke¹⁸ and Alzheimer's disease.^{19–21} However, these particular properties cannot be generalized to all neurological disorders potentially affecting the cerebellum, such as for multiple sclerosis²² or HIV.²³ To avoid a potential bias related to the a priori selection of the anatomical reference region, methods for the automatic extraction of reference region in PET images have been developed over recent years, such as the supervised clustering algorithm (SCA) that was introduced by Turkheimer et al.²⁶ (SuperPk) for [¹¹C]PK11195. The SCA was then validated and used in a [¹¹C]PK11195 multicenter study.²⁷ SCA is based on the creation of a set of predefined kinetic classes that guides the algorithm to select only voxels of no or low specific binding within the brain image.

Recently, a similar SCA approach was successfully applied to other tracers such as [¹¹C]PIB²⁸ or [¹¹C]TMSX.²⁹ An unsupervised clustering approach was also implemented for [¹⁸F]DPA-714 in Amyotrophic Lateral Sclerosis.³⁰ However, no predefined classes were identified and employed to supervise the kinetic shape of the time-activity curves (TACs) in the clusters, and the results were not validated with AIF-derived-2-TCM.

Data from different studies with [³H]PK11195, [¹¹C]PBR28 and [¹¹C]PK11195^{7,24,25} have shown that displaceable binding has a non-negligible contribution

to the distribution volume in the cerebellum. Moreover, recent studies^{31,32} suggest that TSPO is constitutively expressed in several cell types in the brain, including endothelial cells. Given these observations, it may be that there is no brain region entirely devoid of TSPO binding *in vivo*, and the aim here was to validate a method able to define a “pseudo-reference region” that is, tissue with the lowest/basal levels of constitutive TSPO and negligible amounts of microglia. Our objective is to be able to distinguish subjects with and without neuroinflammation due to pathological processes (activated microglia), irrespective of possible methodological bias in the absolute quantification.

In this study, we adapted and validated the SuperPK approach²⁶ to automatically extract the pseudo-reference region from [¹⁸F]DPA-714 images (SuperDPA) in a group of genotyped healthy subjects. The quantification using each reference region method (SCA methods or the a priori anatomically defined cerebellar gray matter) was compared to the AIF-derived 2-TCM quantification described in our previous [¹⁸F]DPA-714 study in the same healthy human subjects.¹⁵ A further validation of the predefined classes for the SCA was performed in three ways. Firstly, the influence of the genetic affinity profile was evaluated. Secondly, the optimal set of predefined classes for SuperDPA was investigated by simulating a set of classes for a range of binding conditions based on the 2-TCM kinetic parameters. Finally, the reproducibility of the SCA method was tested with three subjects who underwent two [¹⁸F]DPA-714 scans.

Material and methods

Subjects

Fourteen healthy volunteers (mean age 46.8 ± 15.7 years, six females) were included from two clinical protocols conducted at the Service Hospitalier Frédéric Joliot and the Institut du cerveau et de la Moelle (NCT02305264 and NCT02319382). Written informed consent was obtained from all participants, and the protocols were approved by the Medical Bioethics Committee of Ile de France Region and in accordance with French legislation and the Declaration of Helsinki 1975 (and revised in 1983). All subjects were considered healthy according to their medical history record and physical examination. They all had a normal brain MRI.

Genomic DNA from blood samples was used to genotype the rs6971 polymorphism of the TSPO gene. The analysis revealed seven HAB (mean age 47.4 ± 16.0 years, three females) and seven MABs (mean age 46.3 ± 16.7 years, three females). No LABs were found among the 14 subjects.

Imaging protocol

Each participant underwent a T1-weighted (T1-w) magnetic resonance image and an [¹⁸F]DPA-714 PET acquisition. More details on the imaging protocols can be found in Lavissee et al.¹⁵ Three subjects (two HABs, one MAB) underwent a second PET acquisition (injected activity difference 30.2 ± 21.6 MBq) after seven to nine days to study the reproducibility of the quantification method.

T1-w imaging was performed using a turbo spin echo sequence (TSE) (TE/TR = 3/6300 ms; alpha = 10, resolution = $0.92 \times 0.92 \times 0.93$ mm) in a 1.5T Philips Achieva (Best, The Netherlands) scanner or an MPRAGE (TE/TI/TR = 2.98/900/2300, alpha = 9°, resolution = $1 \times 1 \times 1.1$ mm) in a 3T Siemens Trio scanner (Erlangen, Germany).

[¹⁸F]DPA-714 was prepared according to standard conditions.³³ Subjects underwent [¹⁸F]DPA-714 PET scans in a high-resolution research tomograph (HRRT, Siemens, Knoxville, TN, USA). After a transmission scan using a ¹³⁷Cs point source, a [¹⁸F]DPA-714 bolus was intravenously injected (198.4 ± 22.9 MBq). The dynamic PET acquisition in list mode lasted 90 min.

Ten subjects (seven HABs and three MABs) out of the 14 included in this study were the same as those described in Lavissee et al.¹⁵ and had AIFs corrected for metabolites.

Image processing

PET acquisitions were corrected for random attenuation and scattered coincidences and reconstructed with the iterative-ordered subset expectation maximization (Ordinary Poisson [OP]-OSEM) 3D method (4 iterations using 16 subsets) including point spread function modeling within the reconstruction (using a 3D Gaussian kernel with 2 mm full-width at half-maximum). Dynamic data were binned into 27 frames (6×1 min, 7×2 min, 14×5 min). Reconstructed dynamic PET data were realigned for motion correction using the frame-to-reference image registration in PMOD 3.5 (PMOD Technologies Ltd., Zurich, CH).

T1-w images were segmented using Freesurfer 5.3 (<http://freesurfer.net>) and regions of interest (ROIs) were selected: thalamus, hippocampus, cerebellar gray matter, white matter and occipital, parietal, frontal and cingulate cortices. A whole brain mask was also extracted. T1-w images and ROIs were resampled into the PET space using a rigid registration in order to extract TACs from each ROI. Data from the left and right hemispheres were averaged. Kinetic modeling (2-TCM) was performed using the COMKAT library and Logan graphical analysis was proceeded using in-house software in Matlab (Math Works, Natick, MA, USA).

Implementation of the supervised clustering algorithm for [^{18}F]DPA-714 (SuperDPA)

As in the SuperPK,²⁶ the SuperDPA algorithm includes three steps to extract the pseudo-reference region: (i) a normalization procedure to scale each frame and make the acquisition comparable across subjects; (ii) the creation of a set of predefined kinetic classes adapted to [^{18}F]DPA-714 for use in the supervised algorithm; and (iii) a supervised clustering algorithm that calculates the contribution of each kinetic class to the signal of each voxel (Figure 1(a)).

Normalization. Each frame is normalized to reduce variability across frames and subjects. The normalization

step is carried out during the definition of the kinetic classes, as well as for each image analyzed using the SCA method. To normalize the scan, the mean value of the activity in the brain in each frame is subtracted from the activity of each voxel in that frame. The resulting “centered” values are divided by the standard deviation of the values over the whole brain at the same frame.

Definition of the kinetic classes of the SuperDPA. Because [^{11}C]PK11195 and [^{18}F]DPA-714 share the same target, we used the same four classes presented by Yaqub et al.²⁷: blood pool class, white matter class, no to low specific binding class (pseudo-reference region) and high specific binding class. The blood

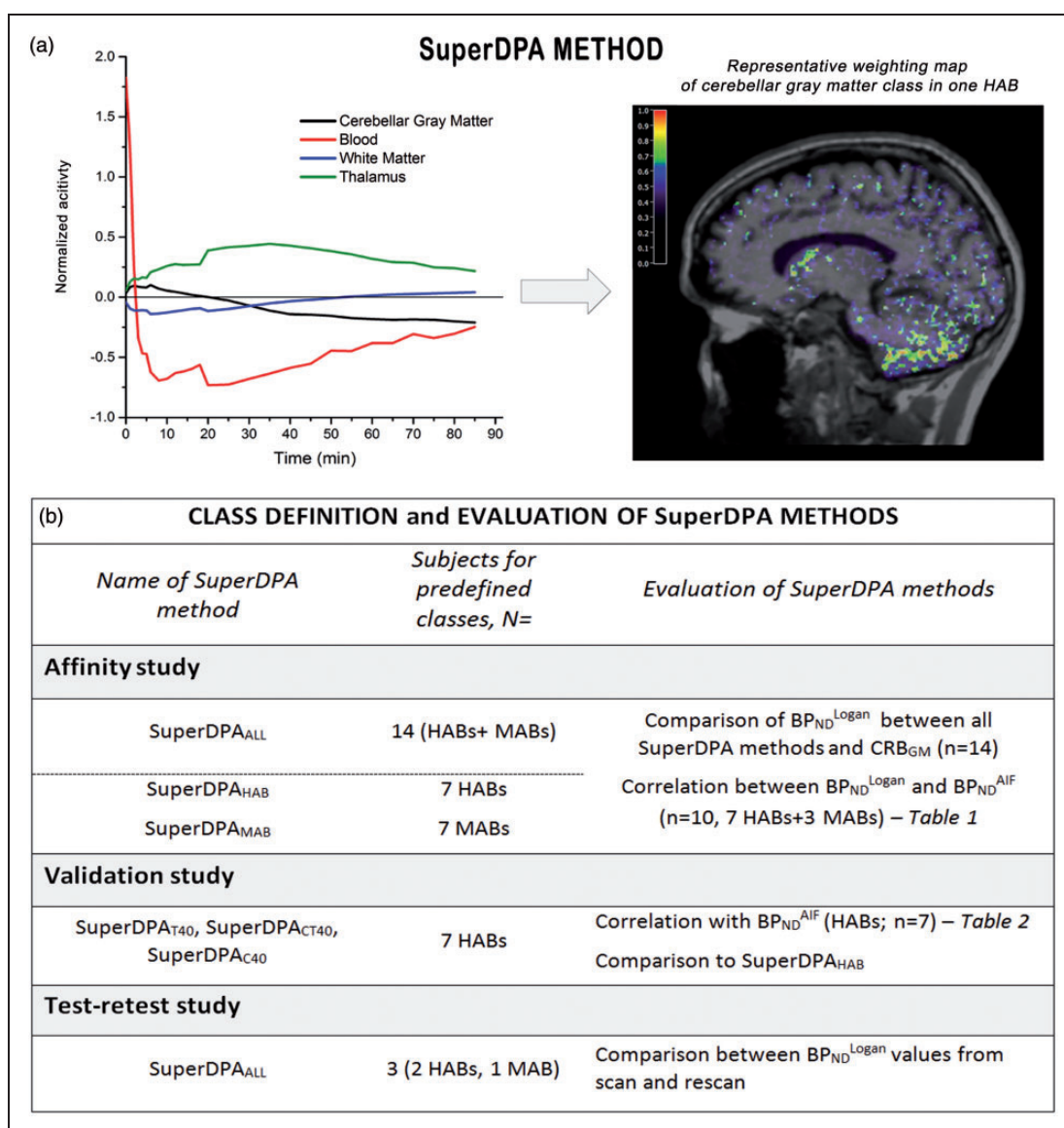


Figure 1. (a) Description of the SuperDPA method and (b) evaluation of this method through affinity, validation and test–retest studies.

pool class was extracted from the carotid arteries that were manually segmented using the PET image summed over the 2 first minutes of acquisition. The white matter class was defined using the Freesurfer automatic segmentation. In healthy controls,¹⁵ the level of binding in the gray matter displayed significant variation, with the highest specific uptake being detected in the thalamus. We therefore chose the thalamus to define the high specific binding class. We chose the cerebellar gray matter (CRB_{GM}) to define the low specific binding class for the following reasons. First, we have previously shown that the lowest binding was found in the CRB_{GM}; second, TSPO mRNA expression was found the lowest in cortical gray matter across brain as derived from Allen Brain Atlas (<http://human.brain-map.org>)³⁴ and finally, Turkheimer et al. observed most voxels of the extracted reference region in the cerebellar gray matter, using SuperPK.²⁶

In each subject, the TACs for each class were then extracted from normalized images (step i) and averaged across the subjects to create the set of classes used for the SuperDPA.

Supervised classification. In order to extract the pseudo-reference region in each PET image, the kinetics of each voxel was projected onto the kinetic classes using a non-negative least squares (NNLS) algorithm, yielding the percent contribution of the each class in that voxel. Voxels in which the TAC was at least 90% attributable to the pseudo-reference were accepted into the binary mask for the pseudo-reference region. The TAC from the pseudo-reference region is a simple average over all the TACs from the voxels included in the binary mask.

Validation of kinetic classes definition

Based on SuperDPA methodology, we developed two different approaches to validate the predefined classes. The first approach assumed that the kinetics of [¹⁸F]DPA-714 depends on the TSPO affinity profile of each given subject. Classes were therefore independently created for HAB and MAB subjects in a so-called “affinity study.” The second approach, a “validation study,” used simulated predefined classes with different characteristics to investigate whether using classes with higher or lower specific binding would yield a more appropriate reference curve (Figure 1(b)).

Affinity study. We investigated the impact of the genetic binding profile of the subjects on the shape of the classes and consequently on the extracted reference curves and estimated parameters. We therefore defined separate sets of classes based on the genetic affinity profiles: classes were created using either the seven MABs, yielding the SuperDPA_{MAB} method to process

the MAB subjects or the seven HABs subjects, yielding the SuperDPA_{HAB} to process the HABs only. For comparison, we also generated a single set of classes from both HAB and MAB subjects pooled together (n = 14), yielding the SuperDPA_{ALL} applied on all subjects, whatever their genetic profile.

Validation of the classes. We generated two types of simulated classes: (1) a simulated reference region class with less specific binding than in the initial CRB_{GM} TAC and (2) a simulated high specific binding class with higher specific binding (from the thalamus TAC). To create the simulated classes, we modified the k_3 parameter previously determined in Lavissee et al.¹⁵ using the 2-TCM. To generate the simulated CRB_{GM} class with lower specific binding for each subject, the initial k_3 of the cerebellum gray matter was decreased by -40%, while all other parameters (K_1 , k_2 , k_4) remained unchanged. Similarly, to generate a simulated higher specific binding class, the initial k_3 was increased by +40%. Again, this was done for each subject. The resulting simulated TACs were used to create the classes for the pseudo-reference region class and the high specific binding class using the method described earlier. For each simulation, the white matter and the blood classes were kept the same as in SuperDPA_{HAB}. For these simulations, the comparison with AIF-based quantification was made within the same genetic profile, and therefore only the HAB group was used (n = 7).

In total, three SuperDPA methods were defined in this “validation study”: the SuperDPA_{C40} method with a 40% reduction in the specific binding of the CRB_{GM} (2) the SuperDPA_{T40} with a 40% increase in the specific binding of the thalamus and (3) SuperDPA_{CT40} method with both 40% decrease in the CRB_{GM} and 40% increase in the thalamus.

Binding parameter estimation

We previously showed¹⁵ that the model that best described the kinetics of [¹⁸F]DPA-714 was the 2-TCM that was therefore used as ground truth in this study. For each ROI, BP_{ND} was indirectly estimated using the AIF as in previous studies^{26,27} to obtain BP_{ND}^{AIF} with

$$BP_{ND}^{AIF} = (V_{TROI} - V_{T-REF})/V_{T-REF}$$

where V_{TROI} and V_{T-REF} are the total volumes of distribution computed with the 2-TCM for the ROI and the extracted reference region of each method, respectively.

In parallel, [¹⁸F]DPA-714 binding in all ROIs was estimated using the Logan reference graphical method for all SuperDPA approaches and CRB_{GM}³⁵ as

previously described.³⁶ The Logan graphical analysis provided the distribution volume ratio (DVR^{LOGAN}) that was converted into BP_{ND}^{LOGAN} ($BP_{ND}^{LOGAN} = DVR^{LOGAN} - 1$).

BP_{ND}^{LOGAN} parametric images were computed using the extracted pseudo-reference region of the SuperDPA methods to show the distribution of specific binding across the brain for each method.

Method evaluation and validation (Figure 1(b))

Affinity study. BP_{ND}^{LOGAN} values estimated from pseudo-reference regions extracted using SuperDPA_{ALL} and SuperDPA_{HAB/MAB} were cross-compared for each subject ($n = 14$) and compared to the BP_{ND} from subjects with arterial sampling ($n = 10$; BP_{ND}^{AIF}). In addition, BP_{ND}^{LOGAN} from these two methods were also correlated to the BP_{ND}^{LOGAN} obtained for the CRB_{GM}. Comparisons were assessed using the Pearson correlation, intra-class correlation (ICC) and relative error coefficients. Relative error was calculated based on absolute BP_{ND}^{LOGAN} and BP_{ND}^{AIF} values.

Validation of the classes. BP_{ND}^{LOGAN} provided by the SuperDPA_{HAB} and the three sets optimized SuperDPA methods (superDPA_{C40}, superDPA_{T40} and superDPA_{TC40}) were compared to BP_{ND}^{AIF} from the 2-TCM-AIF quantification. The agreement between the methods was measured for each ROI using correlation coefficient, ICC and the relative error between BP_{ND}^{LOGAN} and BP_{ND}^{AIF} .

Test-retest study. The reproducibility of the SuperDPA_{ALL}, SuperDPA_{HAB/MAB} and CRB_{GM} was evaluated using the three subjects who had two PET acquisitions within seven to nine days. Each reference region method was applied for both the first and the second PET exams independently, yielding BP_{ND}^{LOGAN} estimates. The relative error was computed between the BP_{ND}^{LOGAN} measurements from the scan and rescan images.

Statistics

For each of the SCA methods investigated, a set of predefined classes were computed using a leave-one-out approach. Then, the pseudo-reference region for the remaining subject was extracted using the classes created without that particular subject.

All statistics were computed using the freely distributed software R (www.r-project.org). Pearson correlation was used as the correlation coefficient. The ICC measured the absolute agreement between the parameters derived when using the AIF and the reference region quantifications, according to the Shrout and Fleiss convention.³⁷ Coefficient of variation was defined

as the standard deviation (SD) of the BP_{ND}^{LOGAN} estimates of all group subjects divided by their mean. Pairwise comparisons were performed using Mann-Whitney or paired Mann-Whitney, when appropriate. BP_{ND}^{LOGAN} obtained from all methods were compared using a one-way paired ANOVA followed by post hoc Bonferroni corrected Fisher tests. Significance for all tests was set to $p < 0.05$.

Results

Pseudo-reference region extraction using the SuperDPA

Weighting maps were extracted from dynamic [¹⁸F]DPA-714 scans of HAB and MAB subjects, using the SuperDPA_{ALL} and the SuperDPA_{HAB/MAB} approaches. The coefficient maps for blood and white matter kinetic classes displayed expected distributions (*data not shown*). Maps representing high specific binding showed voxels mainly located in the thalamus region. Interestingly, the majority of voxels assigned to the pseudo-reference region (probability higher than 90% of belonging to the reference region class) were located in the cerebellar gray matter and caudate and to some extent throughout the cortical gray matter. Representative probability maps from SuperDPA_{ALL} and SuperDPA_{HAB} are displayed in Figure 2(a) for one HAB subject.

Mean TACs from the pseudo-reference region extracted using SuperDPA_{ALL} and SuperDPA_{HAB/MAB} together with TACs of the CRB_{GM} and thalamus are shown in Figure 2(c). TACs using both SuperDPA_{ALL} and SuperDPA_{HAB/MAB} showed a higher peak and a faster wash-out than that obtained in the cerebellar gray matter and reached the same residual activity at 90 min.

Quantification of PET data

Representative BP_{ND}^{LOGAN} parametric images obtained using the voxel-wise Logan method in one HAB subject (SuperDPA_{ALL}) are shown in Figure 2(b). As expected, the highest specific binding was found in the thalamus.¹⁵ BP_{ND}^{LOGAN} obtained using the SuperDPA_{ALL}, the SuperDPA_{HAB/MAB} and the CRB_{GM} are presented in Figure 3. Among studied ROIs, the highest BP_{ND}^{LOGAN} estimates were found in the thalamus, the parietal, cingulate and frontal cortices. The lowest binding was seen in the white matter and hippocampus. To validate the SuperDPA approach, these BP_{ND}^{LOGAN} estimates were compared to BP_{ND}^{AIF} : correlation coefficients r and ICC values between both parameters were found higher than 0.92 in all ROIs except in the white matter ($r = 0.85$, $ICC = 0.86$) using SuperDPA_{ALL} (Table 1).

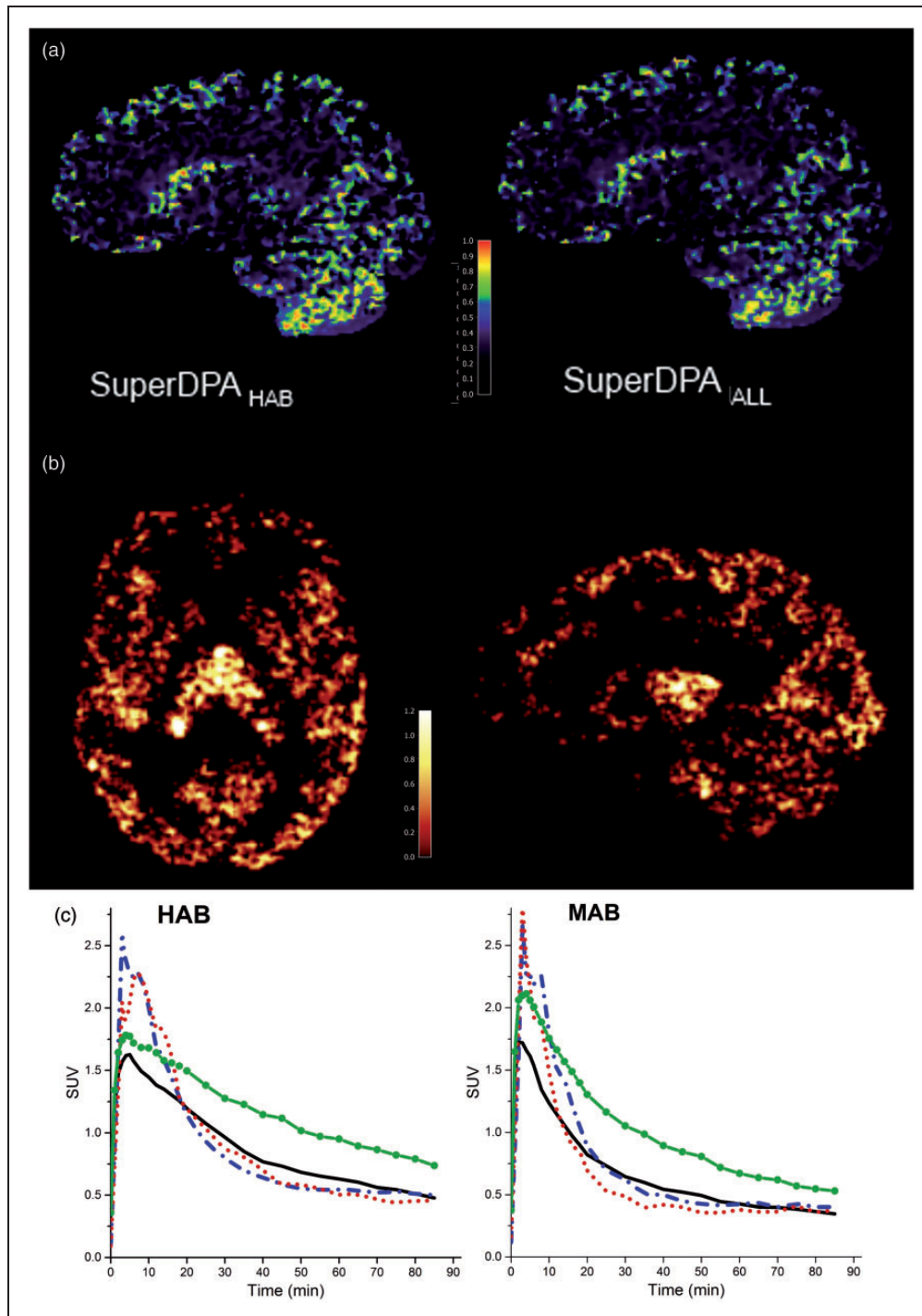


Figure 2. (a) Weighting maps of low/non-specific class (used for reference region selection) for one representative HAB subject using SuperDPA_{HAB} (left) and SuperDPA_{ALL} (right). (b) BP_{ND}^{LOGAN} parametric map (axial and sagittal views) from one HAB subject using SuperDPA_{ALL}. (c) Averaged TACs of thalamus (green line with solid circle), cerebellar gray matter (solid black line) and SCA-based-reference-regions obtained with SuperDPA_{ALL} (dashed blue line) and SuperDPA_{HAB/MAB} (dotted red line) methods. TACs are average SUV from HABs (left, $n = 7$) and MABs (right, $n = 7$).

Influence of the genetic affinity profiles

For all methods (SuperDPA_{ALL}, SuperDPA_{HAB/MAB} and CRB_{GM}), the average TACs of the extracted

pseudo-reference regions showed a slightly different shape between the HAB and the MAB groups (Figure 2(c)). Similar to the CRB_{GM} TACs, both SuperDPA_{ALL} and SuperDPA_{HAB/MAB} could identify TSPO affinity

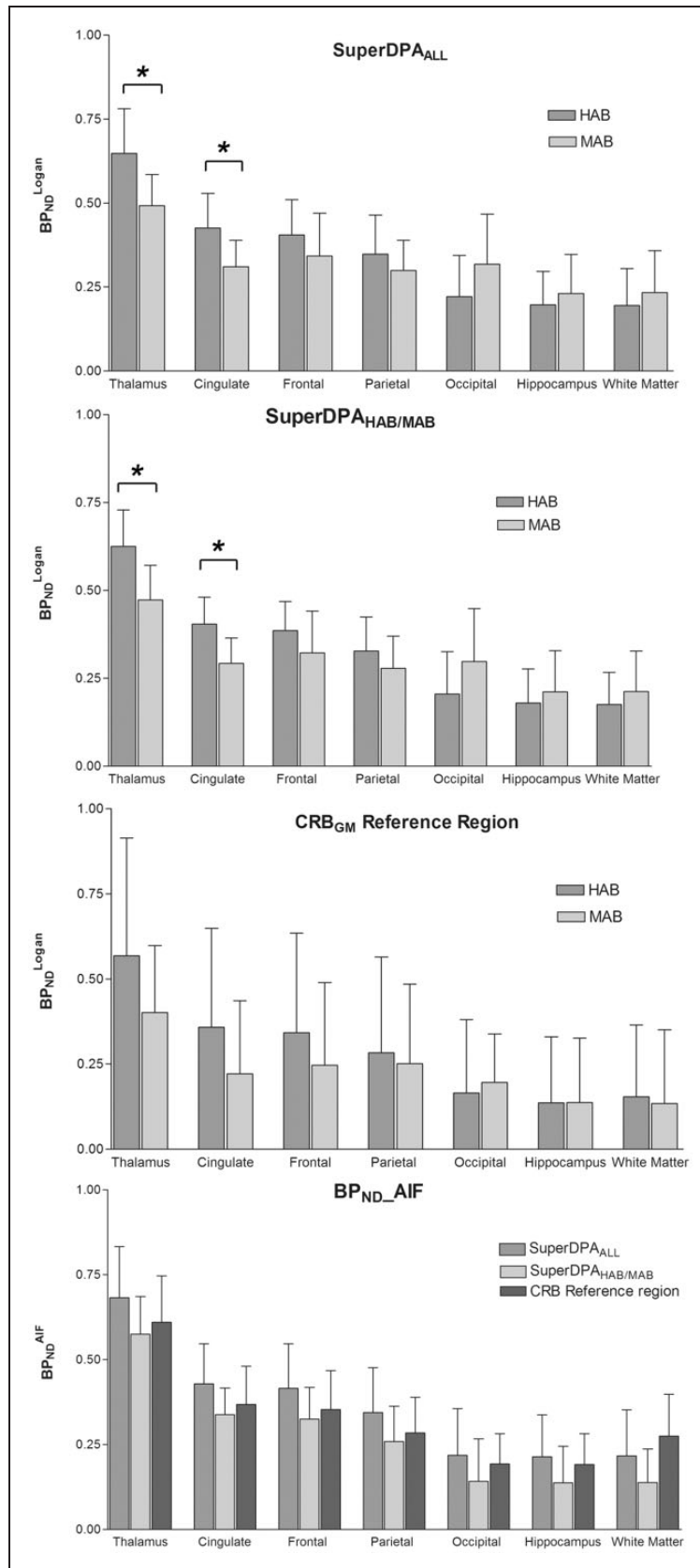


Figure 3. BP_{ND}^{Logan} estimates of each ROI using SuperDPA_{ALL} (top), SuperDPA_{HAB/MAB} (middle) and the CRB_{GM} (bottom) methods in HAB (n = 7) and MAB (n = 7) subjects; BP_{ND}^{AIF} estimates of each ROI using the same methods. Error bars indicate the (SD). *Significant difference, $p < 0.05$.

Table 1. BP_{ND}^{AIF} and BP_{ND}^{LOGAN} correlations using the SuperDPA methods.

	Correlation			ICC			%Relative error			Relative error SD (%)			Regression coeff			
	ALL	HABMAB	CRB _{GM}	ALL	HABMAB	CRB _{GM}	ALL	HABMAB	CRB _{GM}	ALL	HABMAB	CRB _{GM}	ALL	HAB	MAB	CRB _{GM}
Thalamus	0.96	0.96	1.00	0.94	0.92	0.99	-0.53	6.37	-6.73	10.27	7.50	5.86	0.79	0.95		1.07
Cingulate	0.97	0.94	1.00	0.95	0.83	1.00	7.47	15.91	-5.67	19.28	13.69	8.97	0.81	0.97		1.13
Frontal	0.98	0.92	1.00	0.96	0.83	1.00	7.16	16.89	-3.19	19.61	15.08	5.72	0.73	0.97		0.89
Parietal	0.97	0.95	1.00	0.93	0.8	1.00	15.32	27.03	1.22	27.25	17.14	12.72	0.76	1.00		0.96
Occipital	0.90	0.96	1.00	0.88	0.83	1.00	21.95	112.52	106.30	33.86	191.23	294.73	0.79	1.00		0.96
Hipp	0.90	0.96	0.99	0.88	0.88	0.98	15.12	41.41	-6.75	42.20	34.66	47.91	0.69	0.88		0.90
WM	0.87	0.85	0.98	0.83	0.78	0.96	38.66	97.46	-34.32	118.40	170.58	37.28	0.60	0.79		0.78
Mean	0.94	0.93	0.99	0.91	0.84	0.99	15.17	45.37	23.46	38.70	64.27	59.03	0.74	0.94		0.96
SD	0.05	0.04	0.01	0.05	0.05	0.01	12.70	42.38	45.17	36.67	80.33	105.25	0.07	0.08		0.11

Note: Correlation coefficients (r), ICC values, relative error (%), relative error SD (%) and regression coefficients between BP_{ND}^{AIF} and BP_{ND}^{LOGAN} . The latter are estimated using SuperDPA_{ALL}, SuperDPA_{HAB/MAB} and CRB_{GM} ($n = 10$, 7 HABs + 3 MABs). Relative error is calculated against BP_{ND}^{AIF} .

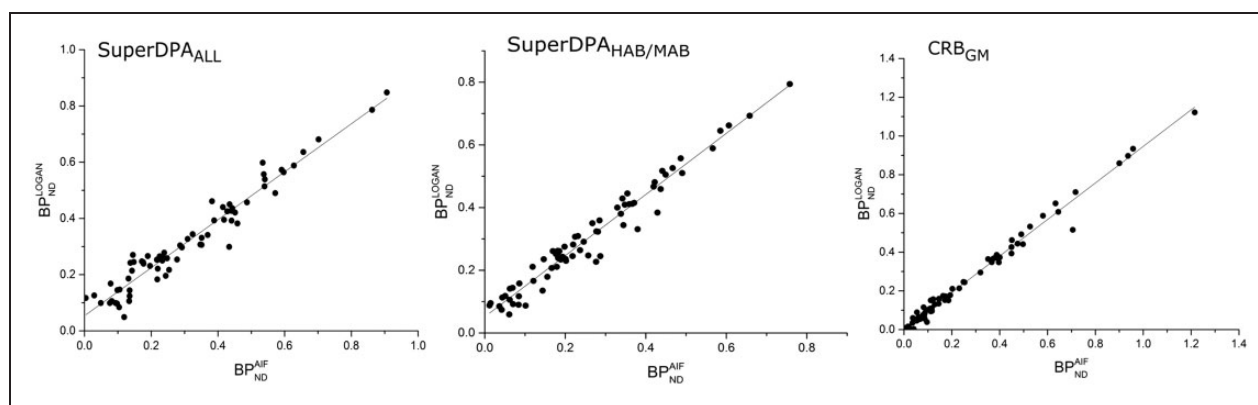


Figure 4. Relationship between BP_{ND} estimates with the arterial input function analysis (BP_{ND}^{AIF}) and with reference input Logan graphical analysis (BP_{ND}^{LOGAN}) using the SuperDPA_{ALL} (left), SuperDPA_{HAB/MAB} (middle) extracted reference region and the CRB_{GM} (right). Regression lines in black lines.

based on the TAC shapes, with a wider peak and a slower wash-out for the HAB group. Using SuperDPA_{ALL}, V_{T-REF} in HABs was found $\sim +28\%$ higher than in MABs ($V_{T-REF} = 3.3 \pm 1.6$ and 2.4 ± 0.07 in HABs and MABs, respectively).

As shown in Figure 3, the mean BP_{ND}^{LOGAN} value was higher in the HAB group compared to the MAB group in the four regions with high specific binding (thalamus and cingulate, frontal and parietal cortices) regardless of whichever pseudo-reference region was used. The difference reached significance in the thalamus and the cingulate cortex when using the supervised clustering approaches only, respectively, $+24.4\%$ and $+27.8\%$ for SuperDPA_{ALL} ($p = 0.04$) and $+24.0\%$ and $+27.0\%$ for SuperDPA_{HAB/MAB} ($p = 0.02$). As illustrated in Figure 3, the BP_{ND}^{LOGAN} using both SuperDPA methods showed much lower standard deviation compared to those obtained with CRB_{GM} in all regions: the

inter-subject variability measured by the coefficient of variation was 0.2 and 0.19 (for HABs and MABs, respectively) using SuperDPA_{HAB/MAB} and 0.17 and 0.21 using SuperDPA_{ALL} compared to 0.61 and 0.49 for the CRB_{GM} reference region. The CRB_{GM} approach did not allow the difference between HABs and MABs to become significant in any region.

For all methods, the BP_{ND}^{AIF} and BP_{ND}^{LOGAN} were found to be highly correlated (Table 1 and Figure 4): r values were above 0.9 for gray matter ROIs and above 0.85 for the white matter. ICC was also high, slightly higher for CRB_{GM} (mean 0.99 ± 0.01) followed by the SuperDPA_{ALL} (mean 0.91 ± 0.05) and SuperDPA_{HAB/MAB} (mean 0.84 ± 0.05).

According to affinity group, the mean BP_{ND}^{LOGAN} estimates were significantly higher with SuperDPA_{ALL} and with SuperDPA_{HAB/MAB} compared to those obtained with CRB_{GM} method in each ROI (averaged over the

Table 2. BP_{ND}^{AIF} and BP_{ND}^{LOGAN} correlations using simulated classes.

	SuperDPA _{ALL}	T ₄₀	C ₄₀	CT ₄₀
Thalamus	0.94 (1.0)	0.95 (3.3)	0.93 (6.9)	0.96 (7.0)
Cingulate	0.93 (4.9)	0.92 (2.4)	0.94 (14.2)	0.97 (13.9)
Frontal	0.94 (6.0)	0.96 (2.8)	0.92 (14.8)	0.96 (14.5)
Parietal	0.95 (4.7)	0.96 (0.7)	0.95 (15.0)	0.97 (14.7)
Occipital	0.97 (13.3)	0.97 (0.2)	0.94 (23.3)	0.97 (21.6)
Hippocampus	0.97 (6.7)	0.93 (22.5)	0.93 (11.0)	0.95 (10.5)
White matter	0.85 (10.7)	0.85 (13.1)	0.89 (12.7)	0.93 (11.5)

Note: Correlation coefficients (and relative errors in %) between BP_{ND}^{AIF} estimates and BP_{ND}^{LOGAN} obtained with SuperDPA_{ALL}, SuperDPA_{T40}, SuperDPA_{C40}, SuperDPA_{CT40} (n = 7 HABs) in all studied ROIs.

seven ROIs, respectively, $+25.6 \pm 10.6\%$; $p < 0.0002$ and $+20.4 \pm 10.6\%$; $p < 0.006$ compared to CRB_{GM}). Furthermore, the mean BP_{ND}^{LOGAN} estimates obtained with all SuperDPA methods overestimated the BP_{ND}^{AIF} values ($+15.2\%$ and $+45.4\%$, respectively – see Figure 4). Interestingly, this relative error was lower in ROIs characterized by a high specific binding such as the thalamus (-0.5% and $+6.4\%$), the frontal cortex ($+7.2\%$ and $+16.9\%$), and the cingulate cortex (7.5% and 15.9%) for SuperDPA_{ALL} and SuperDPA_{HAB/MAB}, respectively. Using the CRB_{GM} as pseudo-reference region resulted in a wider range of relative error from -106.3% to $+34.3\%$ with overall higher absolute values. The standard deviation of the relative error was lower for SuperDPA_{ALL} ($+38.7\%$) compared to other methods (Table 1).

Validation of the predefined classes

The relative errors were found to be different and of greater magnitude in many regions especially when k_3 was decreased for the low binding class (R40). Modifying the k_3 parameter in the simulation, however, led to curves with similar shapes (*data not shown*). Correlations and ICC between the BP_{ND}^{AIF} and the BP_{ND}^{LOGAN} estimates were very high for the three simulations tested (SuperDPA_{T40}, SuperDPA_{CT40}, SuperDPA_{C40} – Table 2). The three simulations did not differ ($p > 0.2$) with SuperDPA_{HAB} with regard to the strength of their correlations with BP_{ND}^{AIF} . ICC between the BP_{ND}^{AIF} and BP_{ND}^{LOGAN} was slightly but not significantly lower for the SuperDPA_{C40} (0.86 ± 0.03) when compared to ICC between BP_{ND}^{AIF} and BP_{ND}^{LOGAN} estimates from SuperDPA_{HAB} (0.93 ± 0.03). Likewise, increasing the specific binding in the high binding class (SuperDPA_{T40} and SuperDPA_{CT40}) resulted in a similar ICC compared to the SuperDPA_{HAB} (0.93 ± 0.03 and 0.90 ± 0.03). Overall, very high agreement between BP_{ND}^{LOGAN} and BP_{ND}^{AIF} was found in all ROIs.

Test–retest study

With respect to the scan–rescan reproducibility, the SuperDPA methods showed a lower average absolute variability compared to the CRB_{GM} (CRB_{GM} : 6.3% , SuperDPA_{HAB/MAB} and SuperDPA_{ALL}: 4.5% – Figure 5) with similar standard deviation around 3.5% for all methods. Interestingly, regions with high specific binding (thalamus, cingulate, frontal and parietal cortices) displayed better reproducibility measures when using SuperDPA methods compared to the CRB_{GM} .

Discussion

In this study, we adapted a supervised clustering approach to automatically extract pseudo-reference regions within the brain from dynamic [^{18}F]DPA-714 PET scans of healthy volunteers. This method provides a non-invasive quantification that has the potential to greatly simplify the use of this tracer in the clinical setting. The quantification performed using SuperDPA showed a very high agreement with the gold standard AIF quantification and a very low inter- and intra-subject variability. We found that the creation of the set of predefined classes using both HAB and MAB subjects is adequate to extract a pseudo-reference region, as it provided results with the same level of reliability than with the creation of two separate sets of predefined classes.

The SuperDPA method was found to be robust for the identification of voxels belonging to the pseudo-reference, i.e. tissue with the lowest levels of constitutive TSPO and the most negligible amount of microglia. This was further validated when the input regions to the SuperDPA classes were compared with optimized set of classes. Although these new classes were based on simulations from the 2-TCM quantification with lower or higher specific binding, they did not impact the correlation with BP_{ND}^{AIF} estimates.

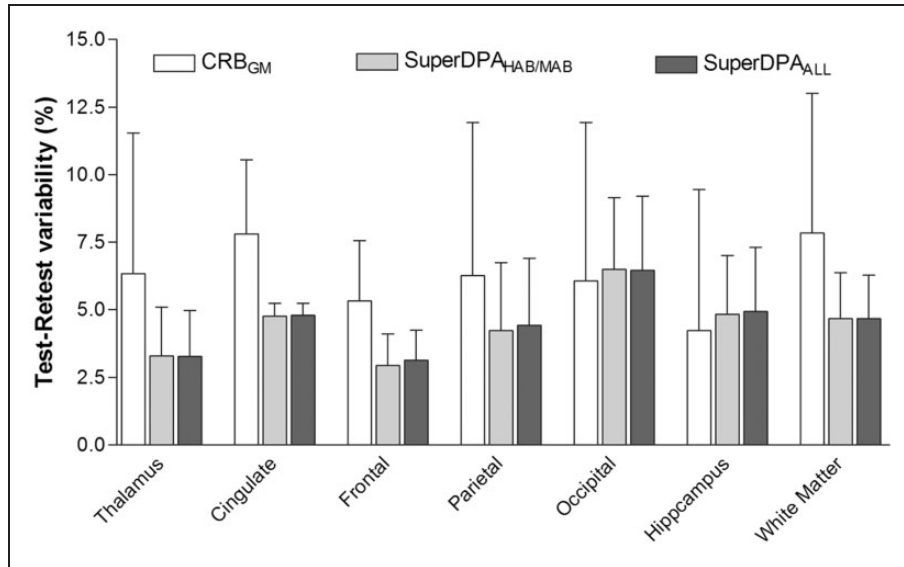


Figure 5. Evaluation of intrasubject-variability (test-retest) of the [¹⁸F]DPA-714 scan measures of each ROI using CRB_{GM}, SuperDPA_{ALL} and SuperDPA_{HAB/MAB} methods. Test-retest variability is calculated as the absolute value of the difference as follows $\text{Variability}(\%) = 100 \times |(DVR_{\text{Test}} - DVR_{\text{ReTest}})| / \text{Mean}(DVR_{\text{Test}}, DVR_{\text{ReTest}})$

We found that the SuperDPA-based quantification had excellent agreement with the AIF-based quantification. Interestingly, correlations of the SuperDPA method with AIF quantification and reproducibility measures were both better in ROIs characterized by high specific binding compared to regions with low binding. This same finding was observed by Collste et al.³⁸ in healthy volunteers and by Park et al. in multiple sclerosis patients compared to healthy controls.³⁹ This suggests that the accuracy and reproducibility of the quantification using SuperDPA should be optimal in pathological conditions associated with a high level of TSPO expression in activated microglia.

The use of CRB_{GM} as pseudo-reference region has previously provided consistent findings for differentiating healthy subjects and Alzheimer patients, at prodromal and dementia stages.^{17,19} This method also showed a strong correlation with AIF quantification among healthy volunteers⁴⁰ as we found in this study. However, only the SuperDPA method should enable to discriminate subtle microglial activation in brain diseases where the location and amplitude of neuroinflammation are unpredictable and may include the cerebellum. The pseudo-reference region extracted from the SuperDPA methods showed a faster wash-out kinetics than the CRB_{GM} and a lower V_T (mean $V_{T-REF} = 3.3 \pm 1.6$ and 2.4 ± 0.07 versus $V_{T-CRBGM} = 3.7 \pm 1.6$ and 2.5 ± 0.04 in HABs and MABs, respectively). This suggests that SuperDPA method could provide reference region TAC closer to the shape of non-displaceable binding than that of the CRB_{GM}. Consequently, SuperDPA provided significantly

higher BP_{ND}^{LOGAN} estimates than for CRB_{GM} ($+25.6 \pm 10.6\%$ and $+20.4 \pm 10.6\%$ for SuperDPA_{ALL} and SuperDPA_{HAB/MAB} compared to CRB_{GM}). We noticed that the V_{T-REF} was higher than the V_{ND} found in our previous paper ($V_{ND} = 0.975$)¹⁵; indeed, the V_{T-REF} corresponds to the pseudo-reference region that includes binding to the constitutive TSPO, whereas the constitutive TSPO is not accounted for in the true V_{ND} calculated with the 2-TCM.

Furthermore, inter-subject variability was found to be lower for SuperDPA than for CRB_{GM} (Figure 3). For both SuperDPA methods, the coefficient of variation of the BP_{ND}^{LOGAN} estimates in the HAB group was of about 33%, which is the same order of magnitude as the V_T estimates in HABs calculated in Lavissee et al.¹⁵ using the AIF quantification in the same subjects. A similar variability was described by Kreisl et al.⁴¹ for the [¹¹C]PBR28 (29-36% for the V_T in HABs) and by Guo et al.⁸ for the [¹¹C]PBR111 (~35% in HABs). However, all these results were obtained using V_T parameter which is related to the global uptake, whereas the BP_{ND} parameter used in the present study should reflect the specific binding more accurately.

The test-retest analysis performed here ($n = 3$) provided a very low BP_{ND} coefficient of variation, less than 7%, for all quantification methods. This coefficient was lower for the SuperDPA approach (4.5%) than for the CRB_{GM} (6.3%), although not significantly. In comparison, poor reproducibility was found using the [¹¹C]DPA-713 in healthy controls by Coughlin et al.⁴² according to a regional V_T systematically increasing from test to retest. For the [¹¹C]PBR28,

Collste et al.³⁸ showed a mean V_T absolute variability of 18% in gray matter and of 48% in white matter in healthy subjects, while Park et al.³⁹ described a test-retest variability between 7 and 9% in healthy volunteers and MS patients. Using the SCA approach and [¹¹C]PK11195, this variation was found of 10.6% in four AD patients.²⁶

Another goal of this study was to take into account the impact of genetic polymorphism related to the affinity of [¹⁸F]DPA-714 to TSPO binding site on the SCA quantification. We confirmed here that the [¹⁸F]DPA-714 binding parameters estimated are affected by the affinity binding status of each subject, similar to the other second generation TSPO tracers.⁸ First, the V_T estimates of the pseudo-reference region extracted were 28% higher in HABs compared to MABs. Likewise, the difference between HABs and MABs was high in TSPO-rich regions: BP_{ND}^{LOGAN} was significantly higher of ~26% in thalamus and cingulate in HABs compared to MABs. This difference is comparable to previous studies: using the 2-TCM in the same subjects, Lavisse et al.¹⁵ found approximately +30% difference in [¹⁸F]DPA-714 V_T in the thalamus. The [¹⁸F]FEPPA tracer was shown to induce either a 27% difference in V_T (with the highest difference in TSPO-rich ROIs)⁴³ or a 15% difference (non-significant) in white matter.⁴⁴ For [¹¹C]PBR28, Kreisl et al.⁴¹ found SUV ~40% greater in HAB subjects than in MAB subjects.

The ability of the SuperDPA method to detect the impact of the TSPO polymorphism on [¹⁸F]DPA-714 uptake finally confirms the superiority of this method over the CRB_{GM} which failed to show a significant difference in binding parameters between HABs and MABs.

Compared to SuperDPA_{HAB/MAB}, the BP_{ND}^{LOGAN} values obtained with the SuperDPA_{ALL} were found closer to those obtained with AIF with a lower relative error, indicating that SuperDPA_{ALL} provides binding parameter estimation that is as accurate as SuperDPA_{HAB/MAB}, if not even better. Therefore, the same supervised clustering procedure can be applied for reference voxels extraction in HAB and MAB subjects. Running SCA does not need the prerequisite of TSPO polymorphism knowledge, but we confirm here that TSPO genotype correction is required for cross-sectional comparisons.

One limitation of the study is that our method was only applied to a healthy group of volunteers. However, healthy subjects have a low expression of TSPO throughout brain regions and the quantification is expected to be more challenging than in patients where higher levels of TSPO expression are observed and therefore statistical differences should be more easily detected. Simulating pathological condition here by increasing the specific binding in the

corresponding class (SuperDPAT₄₀) did not change the extracted reference region and resulting binding parameters. This suggests that our method, based on kinetic classes defined in a population of healthy volunteers, can be applied in patients to accurately detect and quantify neuroinflammation. In an ongoing work, our SCA approach has been applied to nine Alzheimer patients and similar extracted pseudo-reference curves as those obtained in our HAB and MAB subjects were found, which shows that the method can extract the pseudo-reference curve consistently (*unpublished data*).

In this study, the contribution of constitutive binding to TSPO within the reference region is accounted for by the modelling. However, the question of whether this can be a confounding factor remains to be assessed. The introduction of an extra irreversible compartment representing this endothelial cell binding on blood-brain barrier in the model (2-TCM-1K) has been showed to enhance the estimation accuracy of the [¹¹C]PBR28 binding parameters.^{16,45,46} In the present study, the validation of the SCA-based parameter estimation methods was done using estimates from our previous quantification study of [¹⁸F]DPA-714 which describes the 2-TCM as an appropriate model. The question of whether it is necessary to include endothelial binding into the AIF-based quantification for [¹⁸F]DPA-714 and whether it needs to be accounted for in simplified modeling methods as for [¹¹C]PK11195^{25,45} is still under investigation.

Conclusion

In this study, we adapted a supervised clustering approach to automatically extract pseudo-reference regions within the brain from dynamic [¹⁸F]DPA-714 PET images of healthy volunteers. The creation of a unique set of predefined classes from both HAB and MAB subjects was shown to be adequate to extract a pseudo-reference region as it provided results with the same level of reliability than when creating two separate sets of predefined classes. Thus, the knowledge of TSPO genetic status is not a prerequisite to run the SCA method but the 30% difference in BP_{ND}^{LOGAN} and V_{T-REF} between HABs and MABs highlights the need to allocate subjects in their genetic affinity status to allow clinical interpretation. The SuperDPA method was validated through (1) simulated kinetic classes, (2) high correlation with results obtained using quantification based on invasive AIF and (3) by showing very low intra-subject variability. Regarding those criteria, the SCA method appeared to be more robust and accurate than the CRB_{GM} reference region method. Moreover, the SCA allows the possibility of a non-invasive quantification that should greatly simplify the use of this tracer in any neurological disorders.

The very good reproducibility and low inter-subject variability suggest that this method might be able to detect subtle changes in TSPO binding on [¹⁸F]DPA-714 images of patients and to measure longitudinal changes in neuroinflammation.

Funding

The author(s) disclosed receipt of the following financial support for the research, authorship, and/or publication of this article: This work was supported by France Parkinson (NCT 02319382), ANR-08-MNPS-016-02 and ANR-10-IAIHU-06(NCT02305264). A grant from “Investissement d’Avenir – ANR-11-INBS-0011” – NeurATRIS, CEA. The sponsor of the NCT02305264 study was AP-HP (Assistance Publique des Hôpitaux de Paris). BB was partly supported by ECTRIMS and Fondation ARSEP. CW was supported by the Eurotalent grant number 600382.

Acknowledgements

The authors would like to thank chemical/radiopharmaceutical, PET physicist and nursing staff of Service Hospitalier Frédéric Joliot for the synthesis of [¹⁸F]DPA-714, patient management and PET image reconstruction. We thank Lena Guillot, Isabelle Rebeix, Sylvie Forlani, and Luce Dauphinot for the genetic analysis.

Declaration of conflicting interests

The author(s) declared no potential conflicts of interest with respect to the research, authorship, and/or publication of this article.

Authors’ contributions

DGL and SL contributed equally to this article.
BS and MB contributed equally to this article.
DGL, MV, FT, BS and MB made substantial contribution to the concept.
DGL, SL, CL, MV, FT, BS and MB made substantial contribution to the design.
SL, BB, PR and MB made substantial contribution to the data acquisition.
DGL, SL, CL, CW and MB made substantial contribution to the data analysis.
DGL, SL, CL, CW, BS and MB made substantial contribution to the data interpretation.
DGL, SL, CL, CW, BS and MB drafted the article.
BB, PR, MV and FT revised critically the article.
All authors approved the last version.

References

- Glass CK, Saijo K, Winner B, et al. Mechanisms underlying inflammation in neurodegeneration. *Cell* 2010; 140: 918–934.
- Venneti S, Lopresti BJ and Wiley CA. Molecular imaging of microglia/macrophages in the brain. *Glia* 2013; 61: 10–23.
- Benavides J, Malgouris C, Imbault F, et al. “Peripheral type” benzodiazepine binding sites in rat adrenals: binding studies with [³H]PK 11195 and autoradiographic localization. *Arch Int Pharmacodyn Ther* 1983; 266: 38–49.
- Vivash L and O’Brien TJ. Imaging microglial activation with TSPO PET: lighting up neurologic diseases? *J Nucl Med* 2016; 57: 165–168.
- Hinz R and Boellaard R. Challenges of quantification of TSPO in the human brain. *Clin Transl Imaging* 2015; 3: 403–416.
- Chauveau F, Van Camp N, Dolle F, et al. Comparative evaluation of the translocator protein radioligands 11C-DPA-713, 18F-DPA-714, and 11C-PK11195 in a rat model of acute neuroinflammation. *J Nucl Med* 2009; 50: 468–476.
- Owen DR, Yeo AJ, Gunn RN, et al. An 18-kDa translocator protein (TSPO) polymorphism explains differences in binding affinity of the PET radioligand PBR28. *J Cereb Blood Flow Metab* 2012; 32: 1–5.
- Guo Q, Colasanti A, Owen DR, et al. Quantification of the specific translocator protein signal of 18F-PBR111 in healthy humans: a genetic polymorphism effect on in vivo binding. *J Nucl Med* 2013; 54: 1915–1923.
- Rusjan PM, Wilson AA, Bloomfield PM, et al. Quantitation of translocator protein binding in human brain with the novel radioligand [18F]-FEPPA and positron emission tomography. *J Cereb Blood Flow Metab* 2011; 31: 1807–1816.
- Fujimura Y, Zoghbi SS, Simeon FG, et al. Quantification of translocator protein (18 kDa) in the human brain with PET and a novel radioligand, (18)F-PBR06. *J Nucl Med* 2009; 50: 1047–1053.
- Varrone A, Mattsson P, Forsberg A, et al. In vivo imaging of the 18-kDa translocator protein (TSPO) with [18F]FEDAA1106 and PET does not show increased binding in Alzheimer’s disease patients. *Eur J Nucl Med Mol Imaging* 2013; 40: 921–931.
- Abourbeh G, Theze B, Maroy R, et al. Imaging microglial/macrophage activation in spinal cords of experimental autoimmune encephalomyelitis rats by positron emission tomography using the mitochondrial 18 kDa translocator protein radioligand [(1)(8)F]DPA-714. *J Neurosci* 2012; 32: 5728–5736.
- Boutin H, Prenant C, Maroy R, et al. [18F]DPA-714: direct comparison with [11C]PK11195 in a model of cerebral ischemia in rats. *PLoS One* 2013; 8: e56441.
- Golla SSV, Boellaard R, Oikonen V, et al. Quantification of 18FDPA-714 binding in the human brain: initial studies in healthy controls and Alzheimer’s disease patients. *J Cereb Blood Flow Metab* 2015; 35: 766–772.
- Lavis S, Garcia-Lorenzo D, Peyronneau M-A, et al. Optimized quantification of TSPO radioligand 18F-DPA-714 uptake in the brain of genotyped healthy volunteers. *J Nucl Med* 2015; 56: 1048–1054.
- Turkheimer FE, Rizzo G, Bloomfield PS, et al. The methodology of TSPO imaging with positron emission tomography. *Biochem Soc Trans* 2015; 43: 586–592.
- Kropholler MA, Boellaard R, Schuitemaker A, et al. Development of a tracer kinetic plasma input model for (R)-[11C]PK11195 brain studies. *J Cereb Blood Flow Metab* 2005; 25: 842–851.

18. Gerhard A, Schwarz J, Myers R, et al. Evolution of microglial activation in patients after ischemic stroke: a [11C](R)-PK11195 PET study. *Neuroimage* 2005; 24: 591–595.
19. Hamelin L, Lagarde J, Dorothee G, et al. Early and protective microglial activation in Alzheimer's disease: a prospective study using 18F-DPA-714 PET imaging. *Brain* 2016; 139: 1252–1264.
20. Kropholler MA, Boellaard R, van Berckel BN, et al. Evaluation of reference regions for (R)-[(11)C]PK11195 studies in Alzheimer's disease and mild cognitive impairment. *J Cereb Blood Flow Metab* 2007; 27: 1965–1974.
21. Lyoo CH, Ikawa M, Liow JS, et al. Cerebellum can serve as a pseudo-reference region in Alzheimer disease to detect neuroinflammation measured with PET radioligand binding to translocator protein. *J Nucl Med* 2015; 56: 701–706.
22. Politis M, Giannetti P, Su P, et al. Increased PK11195 PET binding in the cortex of patients with MS correlates with disability. *Neurology* 2012; 79: 523–530.
23. Garvey LJ, Pavese N, Ramlackhansingh A, et al. Acute HCV/HIV coinfection is associated with cognitive dysfunction and cerebral metabolite disturbance, but not increased microglial cell activation. *PLoS One* 2012; 7: e38980.
24. Doble A, Malgouris C, Daniel M, et al. Labelling of peripheral-type benzodiazepine binding sites in human brain with [3H]PK 11195: anatomical and subcellular distribution. *Brain Res Bull* 1987; 18: 49–61.
25. Schuitemaker A, Kropholler MA, Boellaard R, et al. Microglial activation in Alzheimer's disease: an (R)-[(1)C]PK11195 positron emission tomography study. *Neurobiol Aging* 2013; 34: 128–136.
26. Turkheimer FE, Edison P, Pavese N, et al. Reference and target region modeling of [11C]-(R)-PK11195 brain studies. *J Nucl Med* 2007; 48: 158–167.
27. Yaqub M, van Berckel BNM, Schuitemaker A, et al. Optimization of supervised cluster analysis for extracting reference tissue input curves in (R)-[11C]PK11195 brain PET studies. *J Cereb Blood Flow Metab* 2012; 32: 1600–1608.
28. Ikoma Y, Edison P, Ramlackhansingh A, et al. Reference region automatic extraction in dynamic [11C]PIB. *J Cereb Blood Flow Metab* 2013; 33: 1725–1731.
29. Rissanen E, Tuisku J, Luoto P, et al. Automated reference region extraction and population-based input function for brain [11C]TMSX PET image analyses. *J Cereb Blood Flow Metab* 2015; 35: 157–165.
30. Corcia P, Tauber C, Vercoullie J, et al. Molecular imaging of microglial activation in amyotrophic lateral sclerosis. *PLoS One* 2012; 7: e52941.
31. Cosenza-Nashat M, Zhao ML, Suh HS, et al. Expression of the translocator protein of 18 kDa by microglia, macrophages and astrocytes based on immunohistochemical localization in abnormal human brain. *Neuropathol Appl Neurobiol* 2009; 35: 306–328.
32. Roncaroli F, Su Z, Herholz K, et al. TSPO expression in brain tumours: is TSPO a target for brain tumour imaging? *Clin Transl Imaging* 2016; 4: 145–156.
33. Kuhnast B, Damont A, Hinnen F, et al. [18F]DPA-714, [18F]PBR111 and [18F]FEDAA1106-selective radioligands for imaging TSPO 18 kDa with PET: automated radiosynthesis on a TRACERLab FX-FN synthesizer and quality controls. *Appl Radiat Isot* 2012; 70: 489–497.
34. Hawrylycz MJ, Lein ES, Guillozet-Bongaarts AL, et al. An anatomically comprehensive atlas of the adult human brain transcriptome. *Nature* 2012; 489: 391–399.
35. Logan J, Fowler JS, Volkow ND, et al. A strategy for removing the bias in the graphical analysis method. *J Cereb Blood Flow Metab* 2001; 21: 307–320.
36. Arlicot N, Vercoullie J, Ribeiro MJ, et al. Initial evaluation in healthy humans of [18F]DPA-714, a potential PET biomarker for neuroinflammation. *Nucl Med Biol* 2012; 39: 570–578.
37. Shrout PE and Fleiss JL. Intraclass correlations: uses in assessing rater reliability. *Psychol Bull* 1979; 86: 420–428.
38. Collste K, Forsberg A, Varrone A, et al. Test-retest reproducibility of [(11)C]PBR28 binding to TSPO in healthy control subjects. *Eur J Nucl Med Mol Imaging* 2016; 43: 173–183.
39. Park E, Gallezot JD, Delgado A, et al. (11)C-PBR28 imaging in multiple sclerosis patients and healthy controls: test-retest reproducibility and focal visualization of active white matter areas. *Eur J Nucl Med Mol Imaging* 2015; 42: 1081–1092.
40. Kreisl WC, Lyoo CH, Liow JS, et al. (11)C-PBR28 binding to translocator protein increases with progression of Alzheimer's disease. *Neurobiol Aging* 2016; 44: 53–61.
41. Kreisl WC, Jenko KJ, Hines CS, et al. A genetic polymorphism for translocator protein 18 kDa affects both in vitro and in vivo radioligand binding in human brain to this putative biomarker of neuroinflammation. *J Cereb Blood Flow Metab* 2013; 33: 53–58.
42. Coughlin JM, Wang Y, Ma S, et al. Regional brain distribution of translocator protein using [(11)C]DPA-713 PET in individuals infected with HIV. *J Neurovirol* 2014; 20: 219–232.
43. Mizrahi R, Rusjan PM, Kennedy J, et al. Translocator protein (18 kDa) polymorphism (rs6971) explains in-vivo brain binding affinity of the PET radioligand [(18)F]-FEPPA. *J Cereb Blood Flow Metab* 2012; 32: 968–972.
44. Suridjan I, Rusjan PM, Kenk M, et al. Quantitative imaging of neuroinflammation in human white matter: a positron emission tomography study with translocator protein 18 kDa radioligand, [18F]-FEPPA. *Synapse* 2014; 68: 536–547.
45. Bloomfield PS, Selvaraj S, Veronese M, et al. Microglial activity in people at ultra high risk of psychosis and in schizophrenia: an [C]PBR28 PET Brain Imaging Study. *Am J Psychiatry* 2015; 75: 1112–1121.
46. Rizzo G, Veronese M, Tonietto M, et al. Kinetic modeling using a two-tissue compartment model and an additional irreversible vascular component improves the quantification of [11C]PBR28 brain PET data. *J Nucl Med* 2014; 55: 2020.